RESEARCH ARTICLE

Transparent Conducting Materials

Energy & Environmental Materials WILEY

Room Temperature Wafer-Scale Synthesis of Highly Transparent and Conductive p-Type Sulfur-Doped Copper Iodide

Sungsan Kang, Taehun Kim, Min Jung, Jinhyeok Pyo, Sohyeon Park, Seonyou Park, Junsung Byeon, Hui Gu Lee, Jin Pyo Hong, Sung-Tae Lee, Minseok Kim, Hyoungsoon Lee, SeungNam Cha, and Sangyeon Pak**

The development of high-performance p-type transparent conductors (TCs) is essential for advancing transparent and flexible electronics yet remains a significant challenge due to the lack of effective p-type materials with high hole mobility and sufficiently large work function. Copper iodide (CuI) has emerged as a promising p-type TC due to its wide bandgap (∼3.1 eV), high transparency (>70%), and excellent hole transport properties. However, optimizing its electrical and optical performance requires precise control over its crystallinity and carrier concentration. Here, we present a room temperature, wafer-scale gas-phase synthesis method for sulfur-doped CuI, where sulfur pre-doping significantly enhances crystal quality and carrier mobility while achieving excellent visible-light transmittance (86%), ultra-low sheet resistance (75 Ω sq^{-1}), and a high work function (>5.9 eV), resulting in a record-high figure of merit (95 000 (MΩ)$^{-1}$) among p-type TCs. Our pre-doping strategy yields superior electrical and optical properties without compromising material stability. Furthermore, this scalable and damage-free synthesis method offers a practical pathway for integrating CuI into next-generation transparent electronics, optoelectronics, and flexible devices.

1. Introduction

The advancement of transparent electronics, encompassing a broad spectrum of applications from solar cells to flexible displays and optoelectronic devices, relies on the development of transparent conductors (TCs) that can efficiently conduct electricity while allowing light to pass through with minimal obstruction. Traditionally, the search for high-performance TCs has primarily focused on n-type materials, which are abundant and well-studied, such as zinc oxide (ZnO), indium oxide (In_2O_3), and tin oxide (SnO_2).[1,2] These materials, known for their wide bandgaps and high electron mobility, have set a high benchmark for transparent optoelectronics.[3–5] However, the development of high-performance transparent technologies, ranging from electronic devices to photovoltaics and optoelectronic systems, requires efficient p-type TCs to complement their well-established n-type counterparts. This remains a significant challenge due to the inherent difficulty of achieving both high hole mobility and stable p-type behavior in wide bandgap materials.[6–9]

Copper iodide (CuI), with its wide bandgap of ∼3.1 eV and high transparency in the visible range (>70%), has emerged as a promising candidate for p-type TC applications.[10–12] The attraction of CuI is not just in its optical properties but also in its exceptional hole transport characteristics, with hole mobilities reported to be up to 44 cm^2 Vs^{-1} in single crystal[13] and carrier densities reaching 10^{20} cm^{-3} in doped copper iodide.[14–17] These outstanding electrical properties, combined with its intrinsic stability and ease of processing, make CuI an attractive material for optoelectronic applications. Furthermore, the γ-phase of CuI is thermodynamically stable under ambient conditions, providing an advantage in device fabrication and long-term stability. The synthesis of CuI thin films has been explored through various techniques, including but not limited to spin coating,[18] vapor iodination,[19] liquid iodination,[20] thermal evaporation,[21] sputtering,[14,22] and pulsed laser deposition (PLD),[15,17,23] each with its own set of advantages and challenges.

Despite these promising attributes, realizing the full potential of CuI as a high-performance p-type TC critically depends on effective doping

S. Kang, J. Pyo, S. Park, S. Park, Prof. S.-T. Lee, Prof. M. Kim, Prof. S. Pak
School of Electronic and Electrical Engineering, Hongik University, Seoul 04066, Korea
E-mail: spak@hongik.ac.kr
Dr. T. Kim, M. Jung, J. Byeon, Prof. S. Cha
Department of Physics, Sungkyunkwan University (SKKU), Suwon, Gyeonggi-do 16419, Korea
E-mail: chasn@skku.edu
H. G. Lee, Prof. J. P. Hong
Division of Nano-scale Semiconductor Engineering and Physics, Hanyang University, Seoul 133-791, South Korea
Prof. J. P. Hong
Research Institute of Convergence of Basic Science, Department of Physics, Hanyang University, Seoul 04763, South Korea
Prof. H. Lee
School of Mechanical Engineering, Chung-Ang University, Seoul 06974, South Korea
The ORCID identification number(s) for the author(s) of this article can be found under https://doi.org/10.1002/eem2.70263.

DOI: 10.1002/eem2.70263

strategies that can precisely control carrier concentration while maintaining high crystallinity.[15–17,20,24] Doping plays a central role in enhancing the electrical properties of CuI, yet conventional approaches often involve high-temperature processing steps that are incompatible with flexible substrates and detrimental to film quality.[25] Furthermore, to improve dopant activation and uniformity, post-deposition annealing is typically employed,[26] however, this often leads to reduced crystallinity, increased grain boundary defects, and degraded carrier mobility.[27] Additionally, nonuniform dopant distribution, impurity scattering, and dopant instability can significantly limit both conductivity and optical transmittance.[28–31] These challenges highlight the importance of developing a low temperature, controllable doping method that enables uniform incorporation, preserves structural integrity, and supports scalable fabrication, key factors in enabling the practical implementation of CuI-based optoelectronic and flexible device applications.

Here, we report an innovative, wafer-scale, room temperature gas-phase pre-doping method for synthesizing high-performance sulfur-doped CuI (S-doped CuI) as a p-type transparent conductor (TC). This sulfur pre-doping approach significantly improves crystal quality and enables precise control over carrier concentration through optimized doping levels, achieving a highly desirable balance between optical transparency, electrical conductivity, and structural integrity. Unlike conventional doping techniques, our method ensures uniform sulfur incorporation into the CuI lattice and modulation of hole concentration and optical bandgap while preserving high crystallinity. As a result, the resulting S-doped CuI films exhibit outstanding performance, with visible transmittance of 86%, ultra-low sheet resistance of 75 $\Omega\,sq^{-1}$, a high work function (>5.9 eV), and a figure of merit of 95 000 $M\Omega^{-1}$, surpassing previously reported p-type TCs. This work highlights the importance of the pre-doping strategy and demonstrates the effectiveness of our low temperature, scalable synthesis method for enabling next-generation transparent and flexible optoelectronic devices.

1.1. Wafer-Scale Synthesis and Structural Evolution of S-Doped CuI

The fabrication process of wafer-scale S-doped CuI is illustrated in **Figure 1a**, which involves a three-step gas-phase synthesis under room temperature conditions. In the first step, a thin Cu film is deposited via thermal evaporation. This is followed by sulfurization, where the Cu film is exposed to H S gas, leading to the formation of a sulfur-containing intermediate layer. During the pre-doping process, sulfur ions react with copper, forming a sulfide-based intermediate structure. This reaction occurs as Cu atoms bond with sulfur, resulting in the incorporation of sulfur into the Cu matrix.[32–35] Importantly, the sulfur doping concentration was precisely controlled by adjusting the H S exposure time, enabling systematic tuning of the electrical and optical properties of the final CuI film.[33,36] By carefully varying the exposure duration, the sulfur content was modulated from 2.5% to 10% (S2.5–S10%), and the resulting doping levels were quantified using energy-dispersive X-ray spectroscopy (EDS) analysis, confirming the successful incorporation of sulfur into the CuI lattice (Table S1, Supporting Information).

Finally, the film undergoes iodination in a vapor-phase iodine environment, resulting in the formation of S-doped CuI. Compared with the original Cu film, the S-doped CuI film exhibits a dramatically enhanced optical transparency, clearly revealing the underlying pattern, thereby confirming the successful conversion from opaque metallic Cu to highly transparent S-doped CuI (Figure S3, Supporting Information). This gas-phase pre-doping strategy enables spatially uniform sulfur incorporation prior to CuI crystallization, resulting in enhanced structural uniformity and improved optoelectronic properties. Notably, the optimal doping level of ~2.5% was consistently achieved across various film thicknesses by appropriately tuning the sulfur exposure time, as discussed in Note S2, Supporting Information, demonstrating its general applicability.

1.2. Optical Properties and Morphology Analysis

The optical transmittance of pristine CuI and S-doped CuI films is compared in Figure 1c, revealing that all films exhibit high transparency in the visible range (450–780 nm). This is further demonstrated by an image of a large-area S-doped CuI film on a polyethylene terephthalate (PET) substrate (Figure 1e). Notably, S2.5%-doped CuI exhibits the highest transmittance, exceeding 86%, while films with excessive sulfur concentrations (5–10%) show a slight decrease in transmittance due to increased light scattering and absorption from sulfur-induced defects. Higher sulfur concentrations introduce band tailing effects and localized defect states, increasing sub-bandgap absorption and reducing optical transparency.[37] The relatively high transmittance of the S2.5%-doped CuI film (~86%) can be attributed to a combination of reduced refractive index and a slight optical bandgap widening, both induced by sulfur doping. Increased hole concentration leads to free carrier and band filling effects,[38] which are known to lower the refractive index in doped semiconductors, thereby reducing surface reflection and enhancing visible transmittance. This behavior has been reported in other wide bandgap systems such as doped CdO.[39] However, at higher sulfur concentrations (≥7.5%), the transmittance decreases again, likely due to dopant-induced scattering and a minor narrowing of the optical bandgap. These trends reflect the interplay between beneficial and adverse effects of sulfur incorporation on the optical properties of CuI thin films. This transition from a well-ordered crystalline phase to a mixed state enhances light scattering and absorption, further lowering transmittance.[40] The bandgap characteristics of the films were further examined using Tauc plots (Figure 1d, Note S4, Supporting Information), which demonstrate a gradual shift in optical bandgap energy with sulfur doping. The bandgap narrowing observed at higher sulfur concentrations suggests an alteration in electronic structure due to sulfur incorporation, potentially leading to enhanced carrier concentration.

To evaluate the surface morphology of the films, atomic force microscopy (AFM) was obtained for pristine CuI and S2.5%-doped CuI (Figure 1b). The thickness of the film increases approximately fivefold during the conversion from Cu to CuI (Figure S4, Supporting Information). The S-doped CuI film exhibits a relatively smooth surface, whereas pristine CuI shows an increased surface roughness (Figure S5, Supporting Information). These observations are consistent with enhanced crystallinity in S-doped CuI, which can be advantageous for improving charge transport properties. Also, in S-doped CuI, the presence of sulfur modulates the reaction kinetics by altering the nucleation density and suppressing uncontrolled grain growth. This effect promotes a more homogeneous microstructure, ensuring a denser and smoother surface.[41,42] The results in Figure 1 highlight the successful room temperature gas-phase synthesis of high-performance S-doped CuI with tunable optical and structural properties.

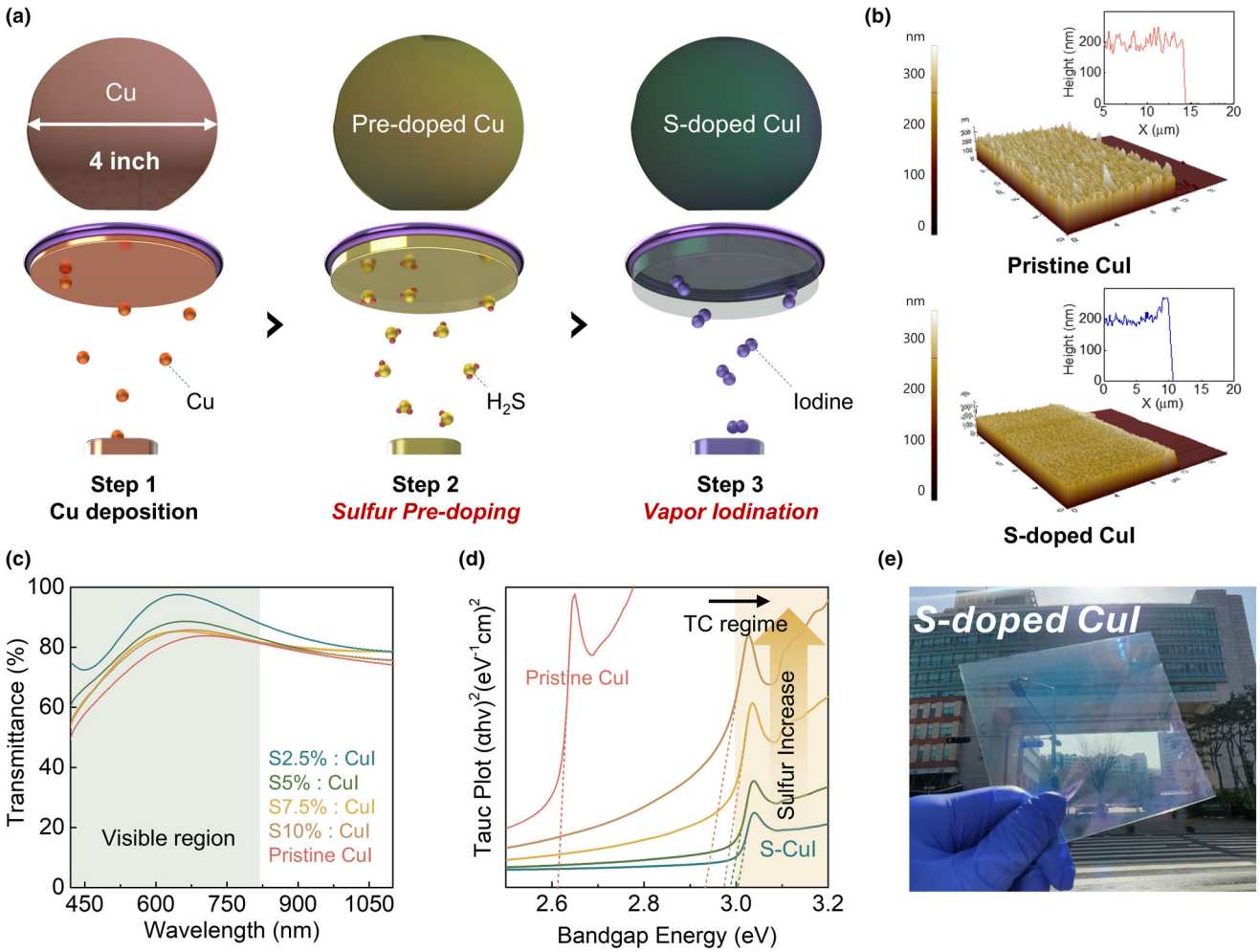

Figure 1. a) Schematic illustration of the scalable fabrication process for sulfur-doped CuI films via room temperature gas-phase sulfur pre-doping followed by vapor iodination. A 4-inch Cu film is first deposited, followed by exposure to H_2S gas for sulfur pre-doping, and finally iodination to yield S-doped CuI. b) AFM images and corresponding height profiles comparing surface morphologies of pristine and S-doped CuI films. c) Optical transmittance spectra of pristine and S-doped CuI films with varying sulfur contents. d) Tauc plots used to extract the optical bandgap of the films. e) Photograph of a large-area (10 cm × 10 cm) S-doped CuI film fabricated on a transparent PET film.

1.3. Chemical and Structural Characterization

To investigate the chemical composition and bonding characteristics of S-doped CuI, X-ray photoelectron spectroscopy (XPS) measurements were performed to investigate the chemical states of the elements (**Figure 2a–c**). In Figure 2a, the Cu 2p spectra exhibit well-defined Cu $2p_{3/2}$ and Cu $2p_{1/2}$ peaks, which remain largely unchanged at low sulfur doping levels. Similarly, the I 3d spectra in Figure 2b show stable iodide bonding and negligible binding energy shift at low doping concentrations, indicating minimal disturbance to the Cu–I bonding environment.[15,20] However, when the sulfur content exceeds 5%, a noticeable downward shift in both Cu 2p and I 3d binding energies is observed. This shift is indicative of p-type doping and can be attributed to an increase in the work function, likely due to changes in the electronic structure and enhanced hole concentration (Figure S6, Supporting Information).[40,41] Figure 2c highlights the S 2p spectra, where the appearance of distinct peaks in doped samples confirms successful sulfur incorporation.[15,20] The increasing intensity of the S 2p peaks with higher sulfur content indicates a systematic doping effect, reinforcing the effectiveness of the gas-phase doping process.

Raman spectroscopy (Figure 2d,e) provides further insight into the structural effects of sulfur doping.[38] In Figure 2d, the Cu-I vibrational mode shows noticeable peak broadening in S-doped CuI, attributed to lattice distortions, increased phonon scattering, and strain induced by sulfur incorporation. Figure 2e reveals an additional S-S vibrational mode, confirming sulfur incorporation and suggesting multiple bonding configurations. These structural changes likely influence the electronic and optical properties of the material.[43] The presence of these peaks suggests that sulfur exists in multiple bonding configurations, including both substitutional sulfur at iodine sites (S_I) and S–S bonded species (e.g., S_2^{2-}). While the latter may reduce the effective hole generation per sulfur atom, the former acts as a shallow acceptor and contributes to increased hole density, as supported by DFT studies.[15] This mixed chemical environment helps explain the observed electrical and optical properties, where increasing sulfur content initially enhances conductivity via increased V_{Cu} formation, followed by saturation or

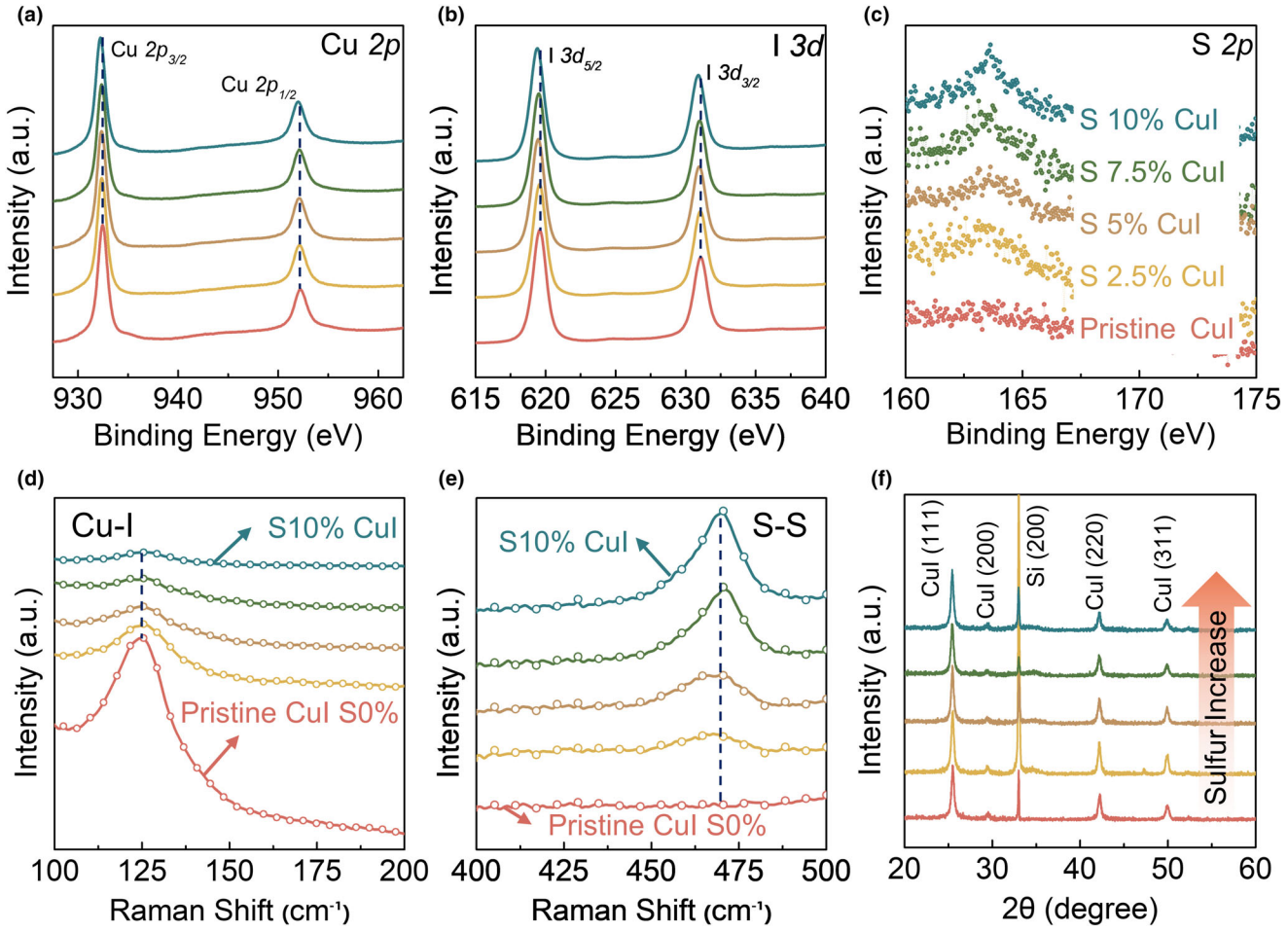

Figure 2. a–c) X-ray photoelectron spectroscopy (XPS) spectra of pristine and S-doped CuI films: a) Cu 2p, b) I 3d, and c) S 2p, confirming successful sulfur incorporation into the CuI lattice. d, e) Raman spectroscopy analysis: d) Cu–I vibrational mode, showing peak broadening with sulfur doping, and e) S–S bonding mode, indicating the presence of sulfur-related species in doped samples. f) X-ray diffraction (XRD) patterns of pristine and S-doped CuI, illustrating phase stability and crystallinity variations with different sulfur doping concentrations.

decline at higher doping levels due to defect clustering or S-S bond formation. These insights help clarify the relationship between Raman-active S-S modes and the observed carrier concentration.

To analyze the crystallographic properties of the films, X-ray diffraction (XRD) patterns were obtained (Figure 2f). The pristine CuI film exhibits strong diffraction peaks corresponding to the γ-phase of CuI, confirming its stable crystal structure. With increasing sulfur content, the primary CuI peaks remain intact, indicating that sulfur doping does not disrupt the fundamental lattice structure. These results indicate that the doping process enhances crystallinity while maintaining the structural integrity of CuI, which is crucial for achieving high-performance TCs. Collectively, XPS, Raman, and XRD analyses verify that sulfur is effectively doped into the CuI lattice without significant structural degradation. The observed changes in bonding, defect states, and lattice parameters demonstrate that sulfur doping can be systematically employed to tailor CuI's electronic and structural properties, an essential step toward optimizing transparent p-type conductors.

To further investigate the impact of sulfur doping on the microstructural properties of CuI, scanning electron microscopy (SEM) and EDS mapping were conducted (**Figure** 3a,b). The top-view SEM images in Figure 3a reveal a significant increase in grain size for S2.5%-doped CuI compared with pristine CuI, suggesting that sulfur incorporation promotes grain growth during the iodination process. The cross-sectional SEM-EDS elemental mapping (Figure 3b) further confirms the uniform distribution of Cu, I, and S, demonstrating successful sulfur incorporation into the CuI lattice without noticeable phase separation.

To quantify the effect of sulfur doping on grain size, the average grain size as a function of film thickness was analyzed (Figure 3c). The average grain size was determined using the Scherrer equation, based on the full-width at half-maximum (FWHM) of the (111) orientation XRD peak for comparison (Table S2). The results indicate that S2.5%-doped CuI exhibits larger grain sizes than pristine CuI at all thicknesses, highlighting the key role of optimal sulfur concentration in enhancing grain growth. This improvement in crystallinity is expected to reduce grain boundary scattering, thereby improving charge carrier transport properties. The relationship between sulfur doping concentration, FWHM of XRD peaks, and grain size was further examined (Figure 3d). The FWHM initially decreases with slight sulfur doping (~2.5%), indicating an increase in crystallinity due to enhanced grain growth. However, at excessive sulfur doping (>5%), the FWHM

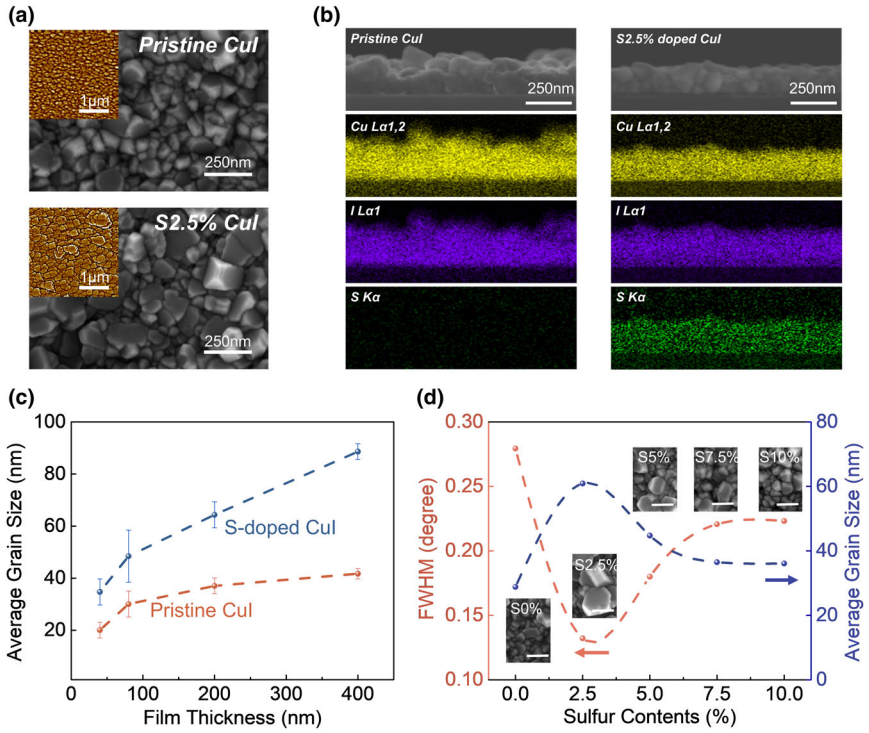

Figure 3. a) Top-view SEM images of pristine CuI and S2.5%-doped CuI, showing grain size differences induced by sulfur doping. Inset images present atomic force spectroscopy images. b) Cross-sectional SEM-EDS mapping of pristine CuI and S2.5%-doped CuI, highlighting elemental distributions of Cu (yellow), I (purple), and S (green), confirming successful sulfur incorporation. c) Variation of average grain size as a function of film thickness, demonstrating enhanced grain growth in sulfur-doped CuI films. d) Relationship between sulfur content, FWHM (full-width at half-maximum), and average grain size, showing a trade-off between crystallinity and grain size with increasing sulfur doping. Inset images represent SEM images with a scale bar of 250 nm.

increases, suggesting increased lattice distortions and defect formation. This trend aligns with the grain size data, where an initial increase in grain size is observed at low sulfur doping, followed by a saturation or slight decrease at higher doping levels due to excessive sulfur-induced disorder. At low sulfur concentrations, sulfur atoms allow sufficient grain growth.[41] This promotes the formation of larger and more uniform grains, reducing grain boundary density and improving charge carrier transport. However, excessive sulfur incorporation introduces significant lattice distortion and internal stress, leading to an increase in nucleation sites while simultaneously inhibiting grain growth. This results in the formation of smaller grains and a higher density of grain boundaries, which ultimately degrade the crystal quality.[44]

1.4. Electrical Properties and Mechanical Stability

To evaluate the effect of sulfur doping on the electrical transport and mechanical stability of CuI thin films, systematic measurements of carrier concentration, mobility, sheet resistance, optical transmittance, and flexibility were conducted. The influence of sulfur doping on the hole concentration and mobility is presented in **Figure 4**a. Sulfur ions substitute iodine sites in the CuI lattice, effectively lowering the formation energy of copper vacancies, the primary source of holes in CuI. This facilitates the formation of additional Cu vacancies, leading to a systematic increase in hole concentration and enhanced p-type conductivity.[15,20,24,45,46]

However, Figure 4b shows that excessive sulfur doping reduces hole mobility due to structural defects and enhanced grain boundary scattering, which impede carrier transport. At excessive doping levels, sulfur accumulation at grain boundaries disrupts the crystal structure and forms localized states that act as potential barriers. While moderate sulfur incorporation promotes grain growth and reduces boundary resistance, excessive sulfur creates scattering centers that hinder mobility. Additionally, defect states introduced into the bandgap act as carrier traps, and increased dopant concentration leads to stronger ionized impurity scattering and lattice strain, further localizing charge carriers. These results highlight the importance of precisely controlling sulfur pre-doping to suppress potential barrier formation and achieve optimal electrical performance.[47–49]

As shown in Figure 4c, the S2.5%-doped CuI film exhibits significantly lower sheet resistance than pristine CuI, particularly in thicker films, indicating improved charge transport due to enhanced grain growth and reduced grain boundary resistance (Note S9, Supporting Information). Figure 4d highlights the trade-off between sheet resistance and transmittance with increasing sulfur content: moderate doping lowers resistance via increased carrier density, while excessive doping reverses this trend due to defect-induced grain boundary scattering.

The enhanced optical transmittance observed in S-doped CuI films can be attributed to a downshift in the valence band maximum (VBM), effectively widening the optical bandgap. The suppression of iodine vacancy defects reduces sub-bandgap absorption and enhances optical transparency in the visible region.[15,20,50] Ultraviolet photoelectron spectroscopy (UPS) measurements further support this observation, showing an increase in work function from 5.6 eV in pristine CuI to 5.9 eV in S-doped CuI (Figure S8, Supporting Information). The shift in the Fermi level toward the valence band edge indicates an increased hole concentration.[38,50] While moderate sulfur doping effectively enhances the p-type conductivity of CuI, excessive sulfur incorporation (typically beyond 5 at%) results in a substantial increase in free carrier concentration. This elevated carrier density intensifies free carrier absorption (FCA), predominantly via phonon and ionized impurity scattering, ultimately leading to reduced optical transmittance.[37] Notably, this combination of a widened optical bandgap, high work function, low sheet resistance, and mechanical flexibility makes S-doped CuI films promising candidates for use as transparent p-type electrodes in advanced optoelectronic applications such as self-powered infrared detectors and piezoelectric nanogenerators.[51–53]

In addition to evaluating their electrical and optical performance, the mechanical flexibility and durability of the S-doped CuI films were investigated through bending tests, as presented in Figure 4ef. S-doped CuI films deposited on polyimide (PI) substrates were subjected to mechanical stability tests under various bending conditions. Figure 4e

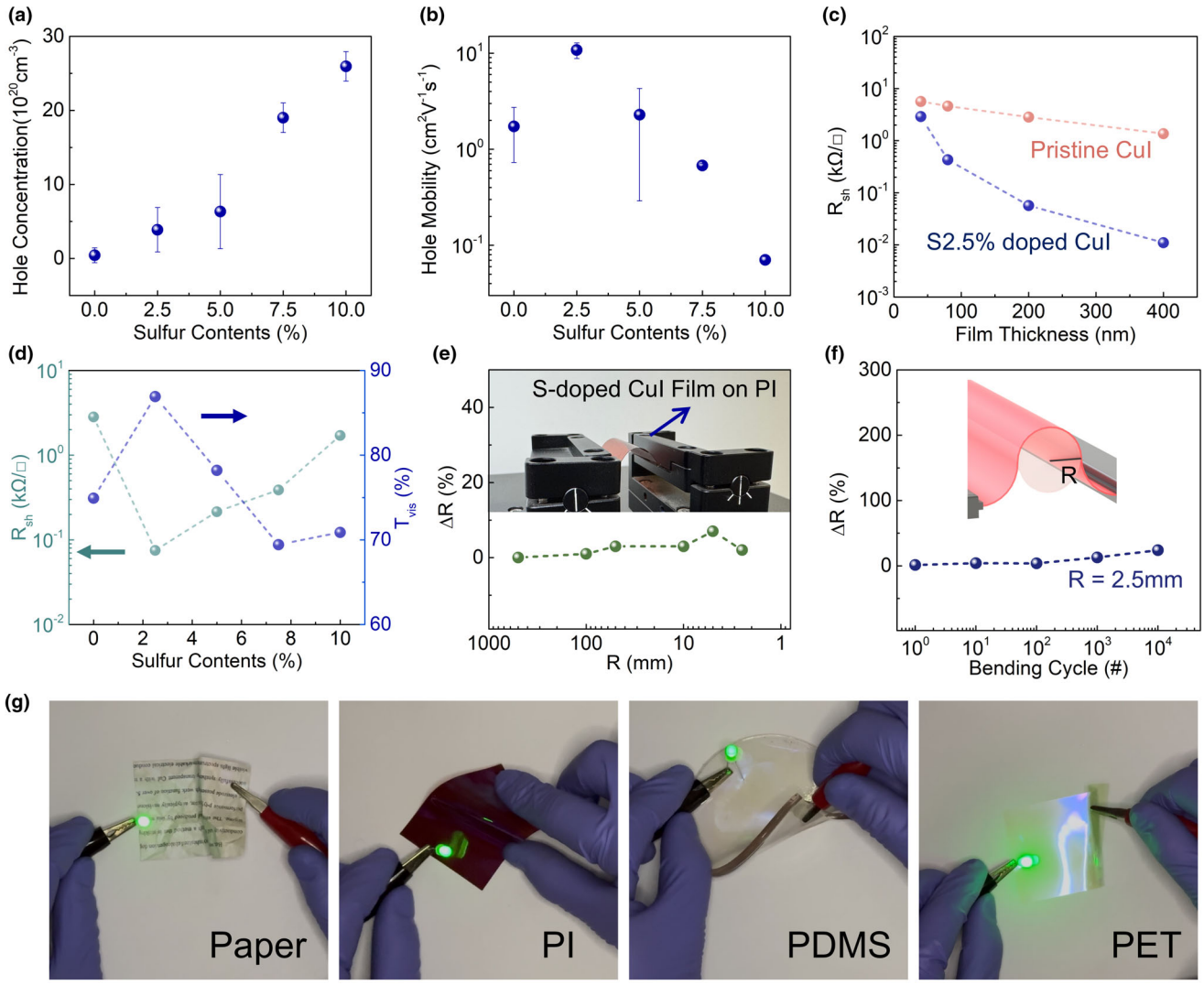

Figure 4. a) Hole concentration and b) hole mobility as a function of sulfur content, illustrating the trade-off between carrier density and transport properties. c) Sheet resistance (R_{sh}) as a function of film thickness, demonstrating the significant reduction in resistance in S2.5%-doped CuI compared with pristine CuI. d) Correlation between sheet resistance and visible transmittance (T_{vis}) across different sulfur doping levels, showing an optimal balance in S2.5%-doped CuI. e) ΔR of S-doped CuI film deposited on a PI substrate as a function of R. f) Mechanical stability assessment through bending tests, showing the ΔR after repeated bending cycles with minimum bending radius of 2.5 mm. g) Photographs of flexible S-doped CuI films fabricated on various substrates (paper, PI, PDMS, PET), highlighting their compatibility with flexible electronics.

illustrates the resistance change (ΔR) as a function of bending radius (R), demonstrating the robustness of the films even when subjected to a bending radius of 2.5 mm. Figure 4f further confirms that the resistance remains stable after 10 000 bending cycles at this radius, highlighting the exceptional mechanical durability and flexibility of the S-doped CuI films.

To demonstrate the versatility of our synthesis method, Figure 4g presents photographs of S-doped CuI films deposited on various flexible substrates, including paper, PI, polydimethylsiloxane (PDMS), and PET. The ability to fabricate high-quality films under ambient conditions at room temperature, regardless of substrate type, underscores the scalability and compatibility of this process for flexible electronics. Notably, such substrate-independent, ambient-condition synthesis is highly relevant in the context of emerging trends in stretchable and self-powered textile electronics.[54–58] The films maintain excellent electrical conductivity and mechanical flexibility, as evidenced by the successful operation of an LED integrated onto these substrates. These results confirm that the pre-doping approach not only enhances the electrical and optical properties of CuI but also enables wafer-scale, room temperature fabrication on soft flexible substrates. This demonstrates the exceptional process scalability and mechanical robustness of S-doped CuI synthesized via pre-doping.

1.5. Figure of Merit Comparison and Technological Implications

The performance of a TC can be quantitatively assessed using the figure of merit (FoM), which is defined as the ratio of electrical conductivity (σ) to the visible absorption coefficient (α). It is expressed as $\sigma/\alpha = -1/[R_{sh}*\ln(T_{vis}+R)]$, where R_{sh} represents the sheet resistance

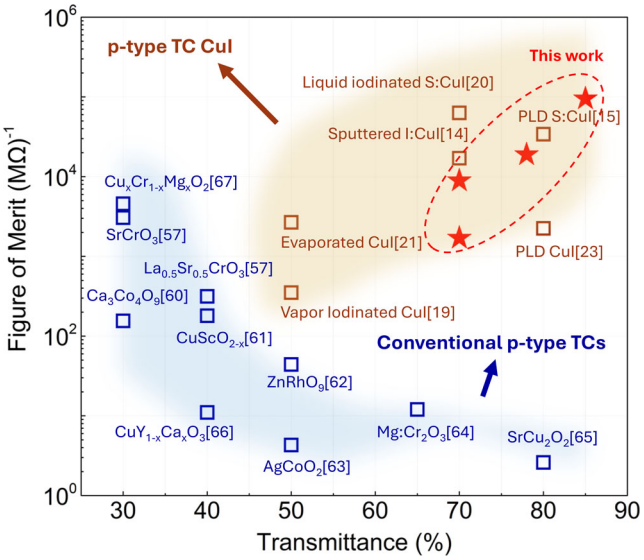

Figure 5. The figure of merit (FoM) is plotted against optical transmittance for various p-type TCs, including conventional oxide-based TCs (blue region) and CuI-based materials (yellow region). Conventional p-type TCs, such as $SrCrO_3$,[60] $Ca_3Co_4O_9$,[61] $CuScO_{2-x}$,[62] $ZnRh_2O_9$,[63] $AgCoO_2$,[64] $Mg:Cr_2O_3$,[65] $SrCu_2O_2$,[66] $CuY_{1-x}Ca_xO_2$,[67] $La_{0.5}Sr_{0.5}CrO_3$,[60] and $CuCr_{1-x}Mg_xO_2$[68] exhibit relatively low FoM values with limited transmittance. However, CuI exhibits a relatively high FoM compared to other p-type transparent conducting materials, including those synthesized via thermal evaporation,[21] pulsed laser deposition (PLD),[23] vapor iodination,[19] and sputtering.[14] The S-doped CuI (This work) and the 3% S-doped CuI fabricated via PLD[15] and S-doped CuI fabricated by liquid iodination[20] are also included for comparison.

($\Omega\,sq^{-1}$) and is given by $1/\sigma d$, with d denoting the film thickness. A higher FoM value indicates superior TC performance.[59] In many studies, due to the absence of R values that represent a reflectance, the FoM is commonly approximated as $FoM = -1/(R_{sh}{*}\ln(T_{vis}))$ by assuming $R = 0$, simplifying the evaluation of TC properties.[14,60]

Figure 5 presents a comparative analysis of the FoM versus optical transmittance for various p-type TCs, highlighting the superior performance of the S-doped CuI films synthesized in this study. The blue-shaded region represents conventional p-type transparent conducting oxides (TCOs), which generally exhibit lower FoM values ($\sim 10^2\,M\Omega^{-1}$) and limited optical transmittance (~30–80%). These materials suffer from inherently low hole mobility and significant intra-grain, which restrict their applicability in high-performance optoelectronic devices due to the trade-off between electrical and optical properties. In contrast, the orange shaded region represents CuI-based transparent conductors, which demonstrate significantly superior FoM values compared with conventional p-type TCOs. Previously reported CuI films synthesized through various deposition techniques, such as thermal evaporation, PLD, vapor iodination, and sputtering-based iodine doping, exhibit improved FoM values in the range of 10^3–$10^4\,M\Omega^{-1}$, with transmittance exceeding 70%.

Among these, the S-doped CuI films fabricated in this study (red stars) exhibit the highest FoM values, underscoring their superior electrical conductivity while maintaining excellent optical transmittance (Table S3, Supporting Information). Notably, the S2.5%-doped CuI sample achieves the highest FoM ($95\,000\,M\Omega^{-1}$) with a transmittance exceeding 85%, representing an improvement over previously reported CuI-based TCs. This enhancement is attributed to optimized grain size, increased carrier concentration, and reduced grain boundary scattering. However, at higher sulfur doping concentrations (>2.5%), the FoM values decline, as evident in the S5% and S7.5% CuI samples.

These findings highlight the effectiveness of room temperature gas-phase sulfur pre-doping in precisely tuning the electronic and optical properties of CuI films. Unlike conventional chalcogen doping methods, which typically require solution-based processing or high-temperature annealing, the pre-doping approach presented here enables uniform sulfur incorporation while maintaining high crystallinity.

2. Conclusions

In this study, we developed high-performance S-doped CuI thin films via a room temperature gas-phase synthesis featuring a controlled pre-doping strategy. This approach enabled uniform sulfur incorporation, enhancing crystallinity, hole transport, and conductivity. Optimized films with ~2.5% sulfur achieved 86% transmittance and a record-high FoM 95 000 $(M\Omega)^{-1}$, while excessive doping (>5%) degraded mobility due to defect formation. The S-doped CuI films developed in this work exhibited high optical transmittance and excellent electrical conductivity while maintaining mechanical stability under 10 000 bending cycles. These properties highlight their strong potential for integration into next-generation self-powered and wearable optoelectronic systems. The scalable, low-cost process makes S-doped CuI a promising candidate for next-generation transparent and flexible optoelectronics.

3. Experimental Section

Detailed information related to the synthesis of active electrodes, physicochemical characterization, and electrochemical evaluation of bifunctional electrodes towards UOR and supercapacitor application is provided in Supporting Information.

Acknowledgements

This work was supported by the National Research Foundation of Korea (NRF) grant funded by the Korea government (Ministry of Science and ICT) (No. RS-2024-00431359 and RS-2024-00411577). This work was also supported by the 2025 Hongik University Innovation Support Program Fund.

Conflict of Interest

The authors declare no conflict of interest.

Supporting Information

Supporting Information is available from the Wiley Online Library or from the author.

Keywords

chalcogen doping, CuI, high work function electrode, p-type electrode

Received: August 18, 2025
Revised: November 18, 2025
Published online: December 2, 2025

[1] X. Yu, T. J. Marks, A. Facchetti, *Nat. Mater.* **2016**, *15*, 383.
[2] D. Won, J. Bang, S. H. Choi, K. R. Pyun, S. Jeong, Y. Lee, S. H. Ko, *Chem. Rev.* **2023**, *123*, 9982.
[3] T. Minami, *MRS Bull.* **2000**, *25*, 38.
[4] C. A. Hoel, T. O. Mason, J.-F. Gaillard, K. R. Poeppelmeier, *Chem. Mater.* **2010**, *22*, 3569.
[5] D. Jayathilake, T. N. Peiris, *SF J. Mater. Chem. Eng.* **2018**, *1*, 1004.
[6] V.-A. Ha, G. Yu, F. Ricci, D. Dahliah, M. J. van Setten, M. Giantomassi, G.-M. Rignanese, G. Hautier, *Phys. Rev. Mater.* **2019**, *3*, 034601.
[7] J. Singh, P. Bhardwaj, R. Kumar, V. Verma, *J. Electron. Mater.* **2024**, *53*, 7179.
[8] Z. Liu, G. Na, F. Tian, L. Yu, J. Li, L. Zhang, *InfoMat* **2020**, *2*, 879.
[9] B. A. Williamson, J. Buckeridge, J. Brown, S. Ansbro, R. G. Palgrave, D. O. Scanlon, *Chem. Mater.* **2017**, *29*, 2402.
[10] M. Grundmann, *Phys. Status Solidi A* **2015**, *212*, 1409.
[11] A. Liu, H. Zhu, M. G. Kim, J. Kim, Y. Y. Noh, *Adv. Sci.* **2021**, *8*, 2100546.
[12] G. H. Kim, J. Lee, K. Ahn, M.-G. Kim, *Soft Sci.* **2024**, *4*, 33.
[13] S. Koyasu, N. Umezawa, J. D. Baniecki, A. Yamaguchi, M. Miyauchi, *Cryst. Growth Des.* **2018**, *18*, 6748.
[14] C. Yang, M. Kneiβ, M. Lorenz, M. Grundmann, *Proc. Natl Acad. Sci. USA* **2016**, *113*, 12929.
[15] A. S. Mirza, M. Pols, W. Soltanpoor, S. Tao, G. Brocks, M. Morales-Masis, *Matter* **2023**, *6*, 4306.
[16] G. H. Kim, H. B. Kim, H. Lee, J. H. Cho, J. Ryu, D. W. Kang, I. Chung, H. Jang, K. Ahn, M. G. Kim, *Small* **2024**, *20*, 2403133.
[17] A. S. Mirza, B. Vishal, P. Dally, C. S. Schnohr, S. De Wolf, M. Morales-Masis, *Adv. Funct. Mater.* **2024**, *34*, 2316144.
[18] A. Liu, H. Zhu, W. T. Park, S. J. Kang, Y. Xu, M. G. Kim, Y. Y. Noh, *Adv. Mater.* **2018**, *30*, 1802379.
[19] F.-L. Schein, H. von Wenckstern, M. Grundmann, *Appl. Phys. Lett.* **2013**, *102*, 092109.
[20] K. Ahn, G. H. Kim, S.-J. Kim, J. Kim, G.-S. Ryu, P. Lee, B. Ryu, J. Y. Cho, Y.-H. Kim, J. Kang, *Chem. Mater.* **2022**, *34*, 10517.
[21] M. Grundmann, F. L. Schein, M. Lorenz, T. Böntgen, J. Lenzner, H. Von Wenckstern, *Phys. Status Solidi A* **2013**, *210*, 1671.
[22] T. Tanaka, K. Kawabata, M. Hirose, *Thin Solid Films* **1996**, *281*, 179.
[23] P. Sirimanne, M. Rusop, T. Shirata, T. Soga, T. Jimbo, *Chem. Phys. Lett.* **2002**, *366*, 485.
[24] J. Willis, R. Claes, Q. Zhou, M. Giantomassi, G.-M. Rignanese, G. Hautier, D. O. Scanlon, *Chem. Mater.* **2023**, *35*, 8995.
[25] M. Imran, R. Ahmad, N. Afzal, M. Rafique, *Vacuum* **2019**, *165*, 72.
[26] M. M. R. Al-Fartoos, A. Roy, T. K. Mallick, A. A. Tahir, *Commun. Eng.* **2024**, *3*, 145.
[27] Y. Shigesato, D. C. Paine, T. Haynes, *J. Appl. Phys.* **1993**, *73*, 3805.
[28] C. Xiao, F. Zhang, Z. Li, S. P. Harvey, X. Chen, K. Wang, C.-S. Jiang, K. Zhu, M. Al-Jassim, *Matter* **2020**, *2*, 261.
[29] V. Zardetto, T. M. Brown, A. Reale, A. Di Carlo, *J. Polym. Sci. B Polym. Phys.* **2011**, *49*, 638.
[30] H. Peelaers, E. Kioupakis, C. Van de Walle, *Appl. Phys. Lett.* **2019**, *115*, 082105.
[31] P. Ščajev, A. Mekys, L. Subačius, S. Stanionytė, D. Kuciauskas, K. G. Lynn, S. K. Swain, *Sci. Rep.* **2022**, *12*, 12851.
[32] S. Pak, J. Son, T. Kim, J. Lim, J. Hong, Y. Lim, C.-J. Heo, K.-B. Park, Y. W. Jin, K.-H. Park, *Nanotechnology* **2022**, *34*, 015702.
[33] T. Kim, S. Pak, J. Lim, J. S. Hwang, K.-H. Park, B.-S. Kim, S. Cha, *ACS Appl. Mater. Interfaces* **2022**, *14*, 13499.
[34] T. Kim, J. Lim, J. Byeon, Y. Cho, W. Kim, J. Hong, S. Jin Heo, J. Eun Jang, B.-S. Kim, J. Hong, *Small Struct.* **2023**, *4*, 2200274.
[35] S. Pak, S. Jang, T. Kim, J. Lim, J. S. Hwang, Y. Cho, H. Chang, A. R. Jang, K. H. Park, J. Hong, *Adv. Mater.* **2021**, *33*, 2102091.
[36] J. Hong, B.-S. Kim, B. Hou, S. Pak, T. Kim, A.-R. Jang, Y. Cho, S. Lee, G.-H. An, J. E. Jang, *ACS Appl. Mater. Interfaces* **2021**, *13*, 4244.
[37] H. Peelaers, E. Kioupakis, C. de Van Walle, *Phys. Rev. B* **2015**, *92*, 235201.
[38] Z. H. Li, J. X. He, X. H. Lv, L. F. Chi, K. O. Egbo, M.-D. Li, T. Tanaka, Q. X. Guo, K. M. Yu, C. P. Liu, *Nat. Commun.* **2022**, *13*, 6346.
[39] C. P. Liu, Y. Foo, M. Kamruzzaman, C. Y. Ho, J. A. Zapien, W. Zhu, Y. J. Li, W. Walukiewicz, K. M. Yu, *Phys. Rev. Appl.* **2016**, *6*, 064018.
[40] F. Geng, Y.-N. Wu, D. Splith, L. Wang, X. Kang, X. Chen, P. Guo, S. Liang, L. Yang, M. Lorenz, *J. Phys. Chem. Lett.* **2023**, *14*, 6163.
[41] R. Heasley, L. M. Davis, D. Chua, C. M. Chang, R. G. Gordon, *ACS Appl. Energy Mater.* **2018**, *1*, 6953.
[42] N. Yamada, R. Ino, Y. Ninomiya, *Chem. Mater.* **2016**, *28*, 4971.
[43] S. Wen, M. Mu, Q. Xie, B. Zhao, W. Song, *Anal. Chem.* **2022**, *94*, 5987.
[44] B. K. Singh, S. Tripathi, *J. Mater. Sci. Mater. Electron.* **2016**, *27*, 2360.
[45] M. Graužinytė, S. Botti, M. A. Marques, S. Goedecker, J. A. Flores-Livas, *Phys. Chem. Chem. Phys.* **2019**, *21*, 18839.
[46] M. Son, G. H. Kim, O. Song, C. Park, S. Kwon, J. Kang, K. Ahn, M. G. Kim, *Adv. Sci.* **2024**, *11*, 2308188.
[47] M. V. Frischbier, H. F. Wardenga, M. Weidner, O. Bierwagen, J. Jia, Y. Shigesato, A. Klein, *Thin Solid Films* **2016**, *614*, 62.
[48] T. Yamada, H. Makino, N. Yamamoto, T. Yamamoto, *J. Appl. Phys.* **2010**, *107*, 123534.
[49] T. Minami, T. Miyata, H. Tokunaga, *Phys. Status Solidi A* **2019**, *216*, 1700783.
[50] J. Wang, J. Li, S.-S. Li, *J. Appl. Phys.* **2011**, *110*, 054907.
[51] W. Li, G. Xie, X. Huo, L. Que, H. Tai, Y. Jiang, Y. Su, *J. Mater. Chem. C* **2025**, *13*, 13582.
[52] X. Luo, B. Liu, W. Li, B. Li, H. Yuan, Y. Su, *Nano Energy* **2025**, *145*, 111438.
[53] X. Luo, W. Li, L. Yuan, G. Xie, Y. Su, *Nano Trends* **2024**, *8*, 100061.
[54] J. Huang, Y. Cai, G. Xie, X. Xu, Z. Geng, Y. Jiang, Y. Su, *Wearable Electron.* **2024**, *1*, 180.
[55] J. Dai, G. Xie, X. Huo, J. Li, S. Deng, Y. Su, *Small* **2025**, *21*, 2407773.
[56] J. Dai, H. Li, G. Xie, L. Que, H. Yuan, Y. Su, *ACS Appl. Electron. Mater.* **2025**, *7*, 7321.
[57] J. Dai, H. Li, L. Que, G. Xie, Y. Su, *Nanoscale* **2025**, *17*, 17345.
[58] Y. Du, S. Kang, Z. Yang, J. Pyo, S. Pak, Y. Cho, *Small* **2025**, *21*, e10367.
[59] R. G. Gordon, *MRS Bull.* **2000**, *25*, 52.
[60] K. H. Zhang, Y. Du, A. Papadogianni, O. Bierwagen, S. Sallis, L. F. Piper, M. E. Bowden, V. Shutthanandan, P. V. Sushko, S. A. Chambers, *Adv. Mater.* **2015**, *27*, 5191.
[61] M. Aksit, S. Kolli, I. Slauch, R. D. Robinson, *Appl. Phys. Lett.* **2014**, *104*, 161901.
[62] N. Duan, A. Sleight, M. Jayaraj, J. Tate, *Appl. Phys. Lett.* **2000**, *77*, 1325.
[63] M. Dekkers, G. Rijnders, D. H. Blank, *Appl. Phys. Lett.* **2007**, *90*, 021903.
[64] J. Tate, M. Jayaraj, A. Draeseke, T. Ulbrich, A. Sleight, K. Vanaja, R. Nagarajan, J. F. Wager, R. Hoffman, *Thin Solid Films* **2002**, *411*, 119.
[65] L. Farrell, K. Fleischer, D. Caffrey, D. Mullarkey, E. Norton, I. Shvets, *Phys. Rev. B* **2015**, *91*, 125202.
[66] A. Kudo, H. Yanagi, H. Hosono, H. Kawazoe, *Appl. Phys. Lett.* **1998**, *73*, 220.
[67] M. Jayaraj, A. Draeseke, J. Tate, A. Sleight, *Thin Solid Films* **2001**, *397*, 244.
[68] R. Nagarajan, A. Draeseke, A. Sleight, J. Tate, *J. Appl. Phys.* **2001**, *89*, 8022.